Geophysical Research Letters

RESEARCH LETTER
10.1029/2021GL092876

Key Points:

- An extended 15 years' observation record of Arctic aerosol light absorbing carbon is employed
- Large-scale circulation patterns appear to induce a long-term modulation in aerosol absorption coefficient (b_{abs}) with regional features
- A 35% increase is found in b_{abs} at Zeppelin during the negative Scandinavian pattern (SCAN) phase in the 6-month cold period compared to the positive SCAN phase

Correspondence to:
K. Eleftheriadis,
elefther@ipta.demokritos.gr

Citation:
Stathopoulos, V. K., Evangeliou, N., Stohl, A., Vratolis, S., Matsoukas, C., & Eleftheriadis, K. (2021). Large circulation patterns strongly modulate long-term variability of Arctic black carbon levels and areas of origin. *Geophysical Research Letters*, *48*, e2021GL092876. https://doi.org/10.1029/2021GL092876

Received 25 FEB 2021
Accepted 9 SEP 2021

Large Circulation Patterns Strongly Modulate Long-Term Variability of Arctic Black Carbon Levels and Areas of Origin

V. K. Stathopoulos[1,2], N. Evangeliou[3], A. Stohl[4], S. Vratolis[1], C. Matsoukas[2], and K. Eleftheriadis[1]

[1]Environmental Radioactivity Laboratory, INRaSTES, NCSR Demokritos, Athens, Greece, [2]Department of Environment, University of the Aegean, Mytilene, Greece, [3]NILU — Norwegian Institute for Air Research, Kjeller, Norway, [4]Department of Meteorology and Geophysics, University of Vienna, Vienna, Austria

Abstract Black Carbon (BC) aerosol is a major climate forcer in the Arctic. Here, we present 15 years (2001–2015) of surface observations of the aerosol absorption coefficient b_{abs} (corresponding to Equivalent BC), obtained at the Zeppelin Observatory, Ny Ålesund, Svalbard, coupled with backward transport modeling with Flexpart in order to calculate the Potential Source Contribution Function (PSCF) for BC. The observed long-term variability superimposed on a strong annual cycle is studied as a function of large-scale circulation patterns represented by monthly index values for the North Atlantic Oscillation (NAO) and the Scandinavian pattern (SCAN). We find a 35% increase of b_{abs} values at Zeppelin during the SCAN$^-$ phase in the winter half-year compared to the SCAN$^+$ phase but no significant difference in b_{abs} values between the NAO index phases. Both NAO and SCAN induce significant regional variability on the areas of origin of b_{abs}, mainly Siberia, Europe, and North America.

Plain Language Summary Here, we investigate the effect of the most important large circulation patterns for the European Arctic, namely the North Atlantic Oscillation (NAO) and Scandinavian (SCAN) patterns on the light absorbing carbon aerosol reaching the highly important area experiencing the effects of climate change as found before. We report important first time findings for an extended observation record of 15 years of aerosol light absorbing carbon, which was never been employed before as a continuous long record, and we performed the first rigorous assessment of the impact of large atmospheric circulation patterns like NAO and SCAN on the transport of black carbon aerosol expressed as the climate relevant aerosol absorption coefficient (b_{abs}) for the first time. We find a significant 35% increase in b_{abs} at Zeppelin during one of the phases of the SCAN. However, a significant regional variability induced by both NAO and SCAN phases is revealed. These findings allow a better quantified estimate of the fate of emissions over the years in the Northern Hemisphere and a better assessment of their influence in the observed BC metrics in the Artic.

1. Introduction

Black carbon (BC) is the second most important climate forcing agent with a net positive radiative effect (Bond et al., 2013). BC aerosols absorb radiation directly and warm the atmosphere, affect cloud formation and cloud lifetime (Garrett et al., 2004; Quaas, 2011), and modify the clouds optical properties (Seinfeld, 2008). BC also interacts with the cryosphere by reducing the surface albedo of snow and ice and intensifying melting (Callaghan et al., 2011; Hadley & Kirchstetter, 2012; Jacobi et al., 2019). BC found in the Arctic is transported mainly from high-latitudes and mid-latitudes through atmospheric pathways with seasonal characteristics governed by the polar vortex. Multi-annual variability of large-scale circulation patterns like NAO may also play a role (Eckhardt et al., 2003; Hirdman, Burkhart, et al., 2010). Emissions of BC are generated by fossil fuel and biomass incomplete combustion. Several modeling studies have simulated the BC annual variation in the Arctic. However, surface concentrations are generally underestimated by models and are in poor agreement with observations (Eckhardt et al., 2015; Sand et al., 2017; Shindell et al., 2008). The reasons for this discrepancy are uncertainties in BC emissions (Stohl et al., 2013; Winiger et al., 2016, 2017), as well as incomplete representation of wet scavenging and transport dynamics in models (Bond et al., 2013; Bourgeois & Bey, 2011). Observational data show declining trends in equivalent BC (eBC)

surface concentrations at most Arctic stations, attributed to emission reductions in certain source areas (Breider et al., 2017; Eleftheriadis et al., 2009). Exploring the impact of general circulation changes on the available long-term observations of Arctic aerosol absorption coefficient (b_{abs}), adds to the understanding of the impact of the climate system variability on BC emissions source areas contributions to Arctic BC concentrations. Information on the causes of long-term variability in b_{abs} and eBC in the high European Arctic derived for different types of atmospheric circulation patterns, can narrow down the uncertainty of long-term forecasts and climate model trends (Collaud Coen et al., 2020; Schmeisser et al., 2018). This work employs long-term observations of the b_{abs} at the Zeppelin station on Svalbard in conjunction with the Flexpart transport model to provide a history of BC transport to this particular receptor, at the center of the European Arctic. The aim of this study is to assess the effect of multi-annual large-scale circulation patterns on light-absorbing aerosol concentration levels and the induced variations in source contributions from different geographical regions during the investigated 15 years.

2. Measurements, Modeling and Statistical Analyses

The data presented here are obtained from aerosol black carbon measurements in the European Arctic at the GAW Zeppelin station, Ny-Ålesund Svalbard (475 m asl; 78°54'N, 11°53'E). Before 2001, data were obtained by means of AE-9 and AE-10 aethalometers (Eleftheriadis et al., 2004). Since 2001 measurements continued until 2019 by means of an AE-31 7-wavelength aethalometer model (Eleftheriadis et al., 2009). Here, the data set from August 1, 2001 to January 1, 2016 are analyzed. A common inlet (snow-hood and stainless steel duct) is used to sample ambient air, which attains laboratory temperature (~20°C) before reaching the aethalometer, hence operation at a relative humidity RH < 20% is ensured. Losses due to diffusion were estimated to be insignificant at <4% due to the high flow rate (>35 lpm) in the inlet duct.

The aethalometer eBC data set for the 880 nm wavelength, is treated according to recent conversion schemes for obtaining aerosol absorption coefficients from light attenuation through loaded filters (Backman et al., 2017). Values are reported for the 880 nm wavelength. Regarding the compensation factor for the multi-scattering effect a value of 3.5 is applied (Backman et al., 2017), while the loading effect is found by a recent study to be insignificant for the high wavelengths of AE-31. Light absorbing carbon or eBC mass concentrations based on the refractory black carbon mass can be obtained from the reported absorption coefficients, applying a Mass Absorption Cross section (MAC) value (6.95 $m^2\ g^{-1}$) derived at the same measurement site for the reported wavelength (Zanatta et al., 2018), while there is further work on the variability of an MAC (Ohata et al., 2021). The b_{abs} reported here is the measured response of arctic light absorbing aerosol (Liu et al., 2020) with the absorption due not only to the associated elemental carbon content of the aerosol but also due to the occasional brown carbon content often present in biomass burning aerosol and the complex microphysical processes leading to absorption enhancement observed for a core-shell aerosol mixing state (Kahnert & Kanngießer, 2020). It is therefore a direct metric relevant to radiative transfer modeling rather than directly representing the initial light absorbing carbon mass (Bond et al., 2013). Screening of measurements for eliminating erroneous data due to instrument malfunctions or local contamination was also conducted based on station logbooks and the quality assurance methodology as described in Laj et al. (2020). The percentage of the 3-h average b_{abs} missing values for the period August 9, 2001–December 31, 2015 is 12.9% (12.5% in the winter period and 13.3% in the summer period). Large-scale atmospheric circulation features are examined through the NAO and SCAN monthly indices downloaded from the website (https://www.cpc.ncep.noaa.gov/) of the Climate Prediction Center (CPC) of the National Weather Service (NWS). The procedure followed for the calculation of the monthly indices is based on the Rotated Principal Components Analysis (RPCA) (Barnston & Livezey, 1987). Although not uniquely defined, the NAO index describes the strength of the pressure dipole, between the Icelandic low and the Azores high (Hurrell, 1995; Hurrell et al., 2003). It extends as far as the mid-latitudes (Hurrell et al., 2003), while its impact is more pronounced in winter than in summer (Folland et al., 2009). In the negative NAO phase, the pressure and height dipole are weakened. The second circulation feature examined is SCAN (Barnston & Livezey, 1987). As the name implies its primary center of action is approximately over Scandinavia, forming a strong anticyclonic positive geopotential height anomaly during its positive phase and a cyclonic negative height anomaly during the negative one.

BC is simulated backwards for 12 days with the Lagrangian particle dispersion model Flexpart (version 9.02) (Stohl et al., 2005), in the so-called "retroplume mode." The model was driven by 3 h 1° × 1° ERA-Interim reanalysis data from the European Centre for Medium-Range Weather Forecasts (ECMWF). The computational domain was resolved at 1° × 1° horizontal resolution and vertically up to 3 km agl. The first level was calculated up to 500 m agl, enough to enclose all types of surface BC emissions. 40,000 computational particles were released every 3 h. The particle release height extended from 25 m below to 25 m above the altitude of the station. For the BC tracer, a density of 1,400 kg m^{-3} was used as in Stohl et al. (2013), while each particle carried a mass size distribution with 0.35 μm mean diameter and 1.25 logarithmic standard deviation at the receptor. Also, the wet deposition parameters were selected according to Stohl et al. (2013). The choices of the simulated distribution and deposition parameters assume a coated relatively hydrophilic particle, as observed during the Arctic haze period (Zanatta et al., 2018).

The Flexpart output is a three-dimensional spatial field (longitude x, latitude y, altitude z) termed Potential Emission Sensitivity (S), with units in nanoseconds per cell. For the lowest vertical level of S, the so-called Footprint Potential Emission Sensitivity (S_F) is obtained. b_{abs} measurements are averaged to fit the model time resolution. .

For processing the model result, we weigh the footprint values S_F in each grid cell according to:

$$S_F'(x,y) = \sum_{t=1}^{n} S_F(x,y,t) \cdot \left(\frac{S_F(x,y,t)}{\tilde{S}_F(t)} \right) \quad (1)$$

In Equation 1 x, y are spatial coordinates and t is the discrete 3-h step of the backward simulation. $S_F(x, y, t)$ constitutes the residence time values of the spatial grid in each 3-h time step. $\tilde{S}_F(t)$ is the median of $S_F(x, y, t)$ at each step. A sequence of weights dependent on the median of the grid at each time step is formed. The median is chosen arbitrarily, as a measure of the residence time magnitude in each time step. The weighing process stresses cells with frequent high residence time values during the backward simulation.

Next, we calculate the response R of the 20% high quantile of b_{abs}:

$$R = \frac{S_{Fh}'}{S_F'} \bullet \frac{1}{\max\left(S_{Fh}'/S_F'\right)} \quad (2)$$

Equation 2 is the well-known Potential Source Contribution Function (PSCF) (Polissar et al., 2001), used for residence time analysis from back-trajectory models. S_F' is the weighted sensitivity of a period and S_{Fh}' is the weighted sensitivity of the 20% high quantile of measured b_{abs} values for the same period. The step-wise weighting process amplifies S_{Fh} more over S_F at grid cells preferred by high measured b_{abs} values. These correspond to source areas and transport pathways related to high b_{abs} values and are represented by the high values of R. Division with the maximum term in Equation 2 is necessary, in order to scale R and retain its probabilistic interpretation. The S_{Fh}' term is empirically filtered from the lowest 25% of its values to avoid spurious R values, occurring from nonsignificant residence times.

3. Results

3.1. Long-Term BC Absorption (b_{abs}) Measurements

b_{abs} measurements at Zeppelin cover almost 15 years (August/2001–December/2015). In Figure 1 the intra-annual variability of 3 h b_{abs} averages for three different five-year periods is shown, namely as 2001–2005, 2006–2010, and 2011–2015. The 5-year periods were chosen empirically as a reasonable length of time over the 15-year data set, in order to examine the overall changes in b_{abs}. For further analyses, we have split the annual cycle in two periods, November–April termed as the "Cold period" and May–October termed as the "Warm period." There is a gradual decrease of b_{abs} values during the Cold period (Table 1) for the three 5-year periods (intra-seasonal median calculated from 3 h averages), which is most evident between the 2001–2005 and 2006–2010 periods. Similar decreasing Cold period trends (Table 1) have been reported by Hirdman, Burkhart, et al. (2010) and Sharma et al. (2013). In contrast, during the Warm period, b_{abs} has been relatively stable, apart from a slight increase of the median by 9.2% in 2006–2010 (Table 1). Table 1 presents the 20% and 80% quantiles for each season and summarizes the basic statistical parameters as well

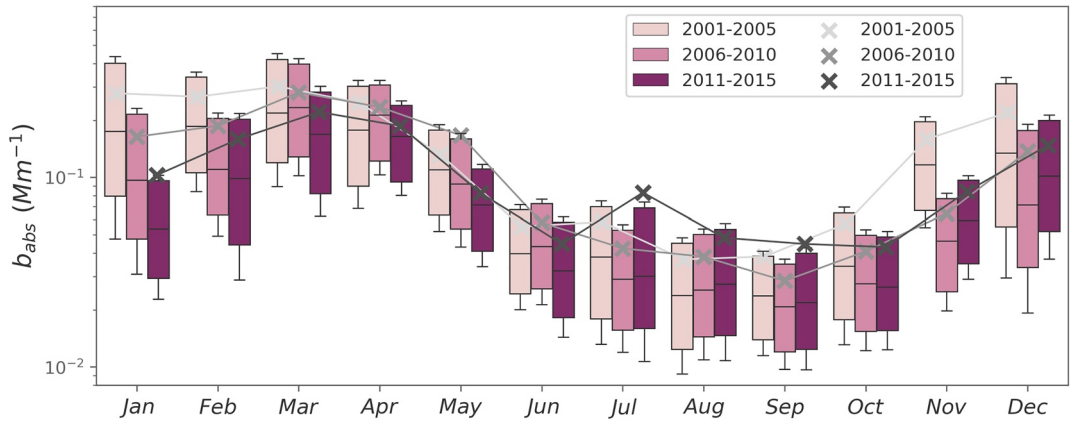

Figure 1. Box-whisker plot of 3 h b_{abs} seasonal averages at Zeppelin, for three different 5-year periods. The 25, 50, and 75 percentiles are shown with boxes while whiskers extend to 10% of the interquartile range of each y axis direction. Cross-marks (x) joined by lines in b_{abs} show the inter-annual means.

as the the mean strength of positive/negative NAO and SCAN indices and their frequency of occurrence for the examined periods. The cumulative anthropogenic (ECLIPSEv6, Klimont et al., 2017) total and open fires (GFED4.1s, Giglio et al., 2013) emission rates are shown over cells that score a PSCF value. Indices strength, frequency, and emission rates are calculated when monthly b_{abs} averages are available.

3.2. Correlation of Large-Scale Atmospheric Circulation Patterns and b_{abs} Observations

We next considered the relation between two important tele-connection indices of the northern hemisphere and b_{abs} measured at Zeppelin. The first is the NAO index (Hurrell, 1995), the most prominent oscilla-

Table 1
Statistics of 3 hr Mean b_{abs} Measurements

b_{abs} Mm^{-1} (eBC ng m^{-3})	Warm period (May–October inclusive)			Cold period (November–April)		
Median	0.035 (7.3)			0.112 (23.4)		
StDEV	0.133 (27.7)			0.202 (42.59)		
80% quantile	0.082 (17.3)			0.293 (61.8)		
20% quantile	0.015 (3.2)			0.046 (9.7)		
	2001–2005	**2006–2010**	**2011–2015**	**2001–2005**	**2006–2010**	**2011–2015**
Median	0.035 (7.3)	0.036 (7.6)	0.033 (6.9)	0.163 (34.4)	0.107 (22.6)	0.100 (21.1)
StDEV	0.078 (16.3)	0.184 (38.4)	0.120 (25.0)	0.239 (50.4)	0.187 (39.0)	0.162 (33.8)
Index strength	**2001–2005**	**2006–2010**	**2011–2015**	**2001–2005**	**2006–2010**	**2011–2015**
NAO^+/NAO^-	0.38/−0.67	0.97/−1.17	0.57/−1.23	0.82/−0.50	0.67/−0.81	1.10/−0.88
$SCAN^+/SCAN^-$	0.73/−0.74	0.77/−0.48	0.86/−0.81	0.86/−0.75	0.63/−0.67	0.80/−0.63
Frequency	**2001–2005**	**2006–2010**	**2011–2015**	**2001–2005**	**2006–2010**	**2011–2015**
NAO^+/NAO^-	11/16	8/19	11/19	15/11	14/14	26/4
$SCAN^+/SCAN^-$	12/14	13/14	14/16	14/12	14/14	14/16
Emission rates	**2001–2005**	**2006–2010**	**2011–2015**	**2001–2005**	**2006–2010**	**2011–2015**
Fossil fuels kg h^{-1} $m^{-2}10^{-6}$	181	181	181	261	282	279
Open fires kg $month^{-1}$ $m^{-2}10^{-4}$	132	466	480	8	18	13

Note. The first four rows show the median, standard deviation (StDEV), upper and lower 20% quantiles of the Warm and Cold periods over the whole b_{abs} series and broken down in the three 5-year periods The next rows are the median and standard deviation of individual periods over the Cold and Warm periods. Values are b_{abs} (Mm^{-1}) and in parenthesis converted to equivalent Black Carbon (see methods, eBC ng m^{-3}). The mean strength of positive/negative NAO and SCAN indices as well their frequency of occurrence and the cumulative anthropogenic (ECLIPSEv6) total and open fires (GFED4.1s) emission rates are also included.

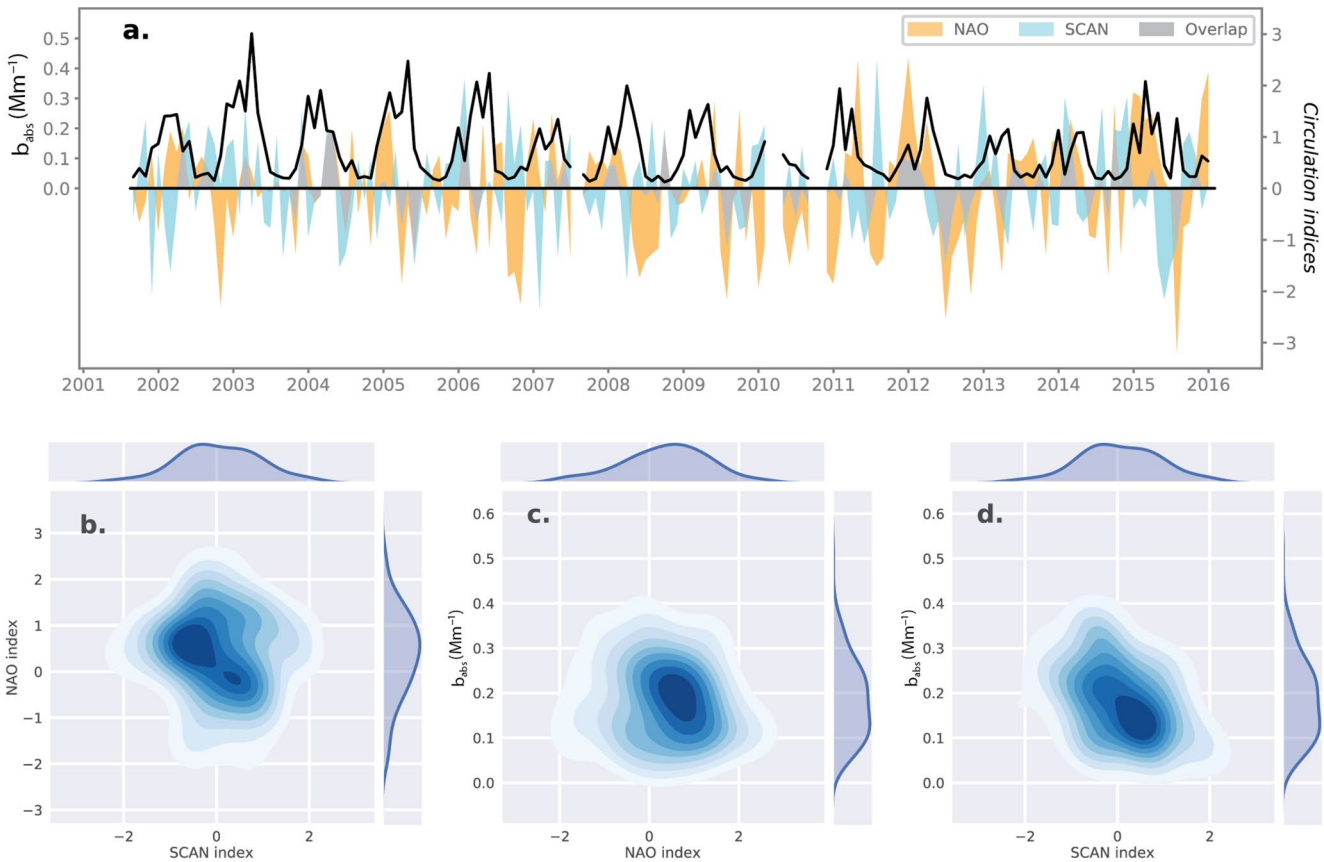

Figure 2. (a) Monthly means of b_{abs} and the corresponding monthly atmospheric circulation indices (North Atlantic Oscillation [NAO], Scandinavian pattern [SCAN]) over the entire period of available measurements. When indices have the same sign, overlap (gray) is used to denote the magnitude of the index with the smaller absolute value. Kernel density scatter plots shown for (b) the circulation pattern indices (NAO, SCAN), absorption coefficient b_{abs} versus (c) NAO and (d) SCAN index for the Cold period.

tion mode of the North Atlantic sector, which is closely related and somewhat embedded in the Arctic Oscillation. Studies of Arctic measurements and model calculations have shown that during positive NAO phases the air pollution concentrations in the Arctic are generally enhanced, due to enhanced northward transport of air masses from Europe and North America (Bacer et al., 2016; Christoudias et al., 2012; Eckhardt et al., 2003). In a previous study (Hirdman, Burkhart, et al., 2010), the variations of NAO over the years were found to have little effect on the overall trend of eBC at Zeppelin. Here, we test this hypothesis on a much longer data set of 15 years instead of 7. It is also important that the parameter evaluated here is b_{abs}, a parameter with lower uncertainty than eBC and closely related to direct radiative forcing.

The second circulation index we study is the Scandinavian pattern (SCAN), due to the role of Scandinavia as a European gateway of air pollution to the Arctic (Hyvärinen et al., 2011; Winiger et al., 2016), the vicinity of Scandinavia to Zeppelin, and the positive correlation of the SCAN index with the blocking activity over Scandinavia and western Siberia (Bueh & Nakamura, 2007). SCAN is usually well developed during the Cold period months (Bueh & Nakamura, 2007), and is mainly negative during the Arctic haze high pollution period for the years in study. From Figure 2a it is observed that NAO and SCAN are usually out of phase with opposite sign as indicated by the small overlap between them. Monthly b_{abs} in the Cold period is higher for $SCAN^-$ (0.211 Mm^{-1} median value) compared to $SCAN^+$ (0.145 Mm^{-1} median value) conditions (Figure 2d). $SCAN^-$ is frequently combined with NAO^+ (Figures 2a and 2b). During the Cold period, the NAO index is more frequently positive. Cold period b_{abs} median is lower for NAO^+ (0.185 Mm^{-1}) than NAO^- (0.201 Mm^{-1}), but NAO^+ is more frequent, in line with Pozzoli et al. (2017). However, when considering the Cold period averages of NAO^- (0.196 Mm^{-1}) and NAO^+ (0.186 Mm^{-1}) the difference is less pronounced. NAO^- is encountered most frequently in the middle 5 years of the Cold period. Overall, the

SCAN$^+$ b_{abs} values are higher with NAO$^-$ (0.56 Mm^{-1} median value) and lower with NAO$^+$ (0.129 Mm^{-1} median value). This can be at least partly attributed to the large frequency of NAO$^+$ during the last period when b_{abs} is generally low (Table 1).

In the Warm period the relationship between b_{abs} and the NAO and SCAN indices is less pronounced. Highest Warm period mean b_{abs} values (0.066 Mm^{-1} mean value) relate with NAO$^-$ at either phase of SCAN. Nevertheless, looking at the individual periods the highest b_{abs} is observed during positive SCAN phases in the middle 5 years (Table 1). Also, b_{abs} and SCAN index values co-vary. These differences are minor and difficult to accurately quantify, considering the low signal-to-noise ratio in the Warm period (Stone et al., 2014).

3.3. Potential Source Areas of b_{asb} Measured at Zeppelin Over the 15-Year Period

The Flexpart BC tracer model was used for simulating backwards the light-absorbing aerosol arriving at Zeppelin. Simulations for 12 days backward in time were used. 12 days can be regarded as a maximum lifetime for the BC (Holopainen et al., 2020; Qi et al., 2017) and though there is not a global BC lifetime, Arctic BC lifetime is generally larger than in other areas (Lund et al., 2018). The wet and dry deposition schemes employed in the model constrain successfully the output for the BC tracer, while allowing robust simulation of aged particles.

We examined the source origin of BC observed at Zeppelin during the 15 years of this study by means of the PSCF of the 20% highest b_{abs} values for the Cold and the Warm periods (Figures 3a and 3b). As source regions, we consider areas in the first model layer, where most emissions occur. Though, one should be aware that when transport pathways intersect and merge over source regions, the PSCF values over the primary sources can be reduced and diffused, while high potential source contribution values can be observed over the pathways. Given a large enough data set, like the one presented here, possibly different pathways from the source regions would dampen high PSCF values along the transport pathways, resulting in the highest PSCF values occurring over the actual BC sources. However, few spurious maxima can still emerge as statistical artifacts, or along the persistent BC transport pathways. We find important Cold period hot spots located over Siberia at the Yamal-Nenets and Khanty-Mansiysk major gas flaring regions (Casadio et al., 2012; Huang & Fu, 2016) (Figure 3a). In a wide domain that includes the industrialized Volga region and northern-western Kazakhstan, the PSCF values are enhanced, indicating important sources mainly over Russia (Figure 3a). Eastern Siberia-Asia displays diffused and relatively lower PSCF values (Figure 3a) as a result of the small BC emissions in the area in the Cold period. Slightly elevated PSCF values appear near 60°N and ~110°–135°E, where some power plants, gas flares, and residential emissions exist (Winiger et al., 2017) and their impact documented (Popovicheva et al., 2017). The elevated PSCF values above the Laptev Sea could be the effect of transport of emissions from north-eastern China (Popovicheva et al., 2019; Winiger et al., 2017), descending in the high Arctic after transport aloft, which is not visible in our PSCF analysis. Hirdman, Burkhart, et al. (2010) also reported an increased pollution transport frequency from East Asia for three high Arctic stations, due to increased regional emissions from these areas. Part of the gas flaring central northern Siberia region shown in the Cold period can also be found as a PSCF maximum in the warm season.

Influence from eastern North America is shown by direct northward transport across the Canadian archipelago (Figure 3a). Over the Atlantic Ocean few localized source areas or pathways are found consisting of two distinct branches, converging toward the south of Greenland (Figure 3a). These features may well represent background BC originating from further south reinforced by gas flaring (e.g., Nova Scotia) and shipping emissions (Marelle et al., 2018). They are also observed to coincide with a NAO$^+$ and SCAN$^-$ pattern. The gas flaring region in Alberta-Northwest Territories is also identified in the Cold period PSCF (Figure 3a). Over North Canada and Alaska, an extended source region is located as a result of large-scale forest fires during the Warm period (Figure 3b). We also show the PSCF results separated in two sub data sets for the Cold and Warm periods (first and second column of Figure 3). The subsets correspond to the values obtained during months with positive and negative SCAN and NAO indices, respectively. The geometric mean values of the highest 20% absorption values for each sub data set used in the analysis, show a similar result in line with the analysis above, where only the SCAN pattern has a pronounced effect (cases c and d). The negative SCAN index is associated with 35% higher aerosol absorption measurements at Zeppelin, while in all other cases the geometric mean values of the highest 20% absorption values show no significant difference (cases e, f, k, l, m, and n).

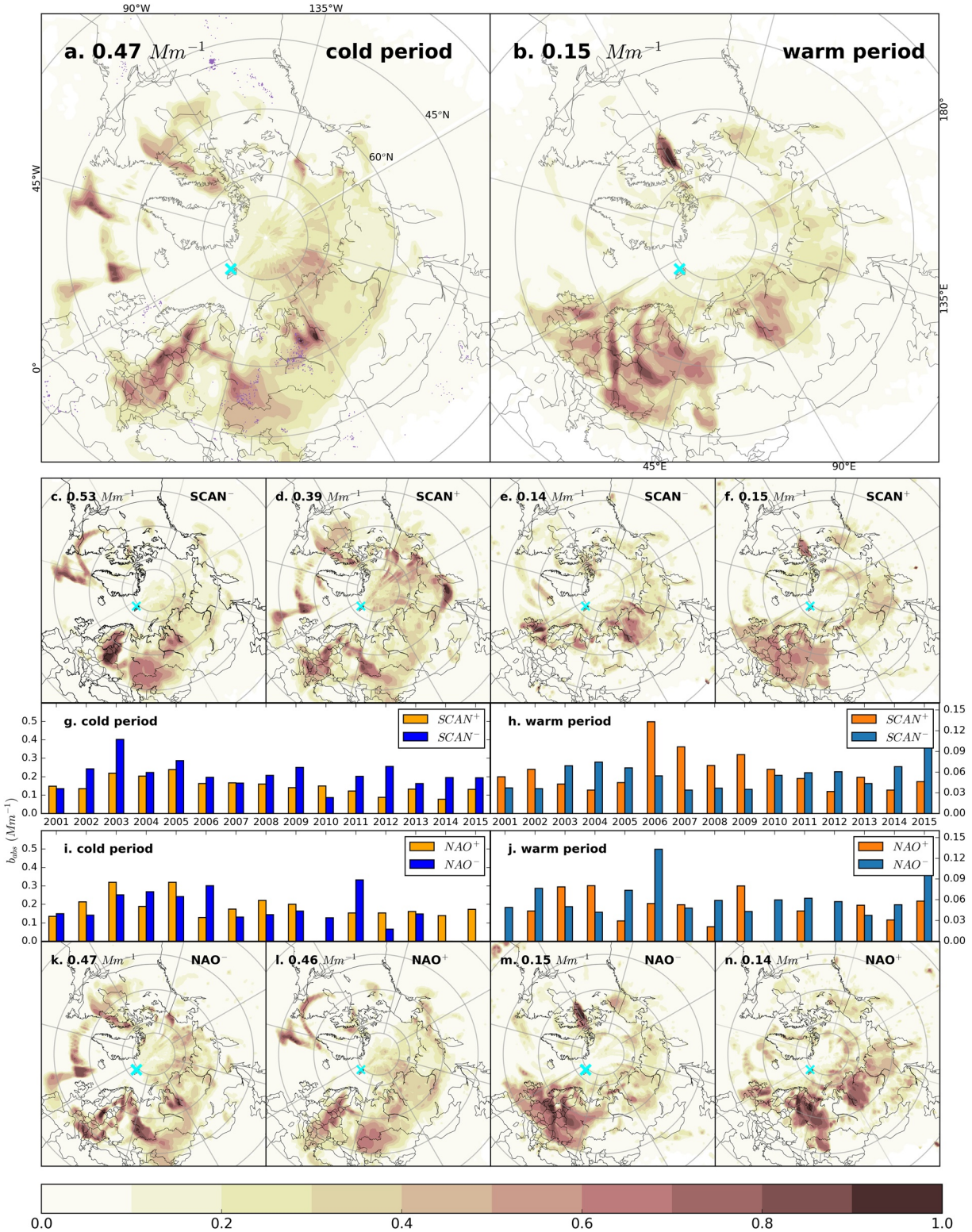

Figure 3. Potential Source Contribution Function (PSCF) based on the Flexpart black Carbon (BC) tracer for the highest 20% of all b_{abs} values measured during the Cold (a) and the Warm (b) periods. In panels (c and d, k and l) we show the PSCF during the Cold period with SCAN⁻, SCAN⁺, NAO⁻ and NAO⁺ respectively. In the panels (e and f, m and n) the corresponding cases for the Warm period are shown. The bar plots display the yearly averaged b_{abs} values, during the Cold (g), (i) and the Warm (h), (j) periods with different signs of atmospheric indices. In the top right corner of each map the geometric mean of the 80% quantile of b_{abs} is displayed. The cyan x symbol indicates the location of the Zeppelin station and the purple dots active gas flares sites (2014).

During the Cold period SCAN$^-$, the source areas are limited to northeastern Europe and the Baltic, large areas of Western Russia and Caspian/Kazakhstan areas as well as the Yamal gas flaring region. On the other hand, when SCAN$^+$ is dominant, the sources in eastern Europe extend much further to the south, while the Russian and Siberian sources are much more diffused across the whole regions to the east, where more source areas appear to play a role. The NAO$^-$/NAO$^+$ Cold periods are not associated with different overall absorption values and the source regions are quite similar. However, the NAO$^-$ period is associated with more localized source areas in Eurasia and a spread of sources from Northwest America, while the opposite is observed during NAO$^+$, where the Eurasian sources are distributed mostly from Central Siberia and westwards. It should be noted that a recent study encompassing data from six arctic sites and for a three-year period has demonstrated that air mass pathways associated with high absorption values in the arctic may originate as far south as the Indian subcontinent (Backman et al., 2021), something not confirmed in the present study and with the Flexpart BC tracer methodology (Petäjä et al., 2020). During the Warm period of the year, some distinct influence of the transport patterns discussed is again visible. It is evident that during the SCAN$^-$ and NAO$^+$, no influence from source areas south of the 60°N is observed across the whole hemisphere. This is associated with a retreating polar front during the Warm period. During the Warm period and under the influence of SCAN$^+$ and NAO$^-$ the source areas are very similar. An important observation here is that the latter index patterns during the Warm period are the only cases when the direct influence of BC source areas from Western Europe is evident. Sources from wildfires in Alaska and Canada are also visible during these cases.

4. Conclusions

Long-term b_{abs} measurements were analyzed from the perspective of variations in large-scale atmospheric circulation patterns. Distinct conclusions are drawn about the source areas, the transport pathways and their efficiency, as they reflect on b_{abs} magnitude at Zeppelin. Essentially, these changes cause modulations on b_{abs} seasonality. The results of the approach can be used as diagnostics in modeling calculations. Furthermore, they point out the importance of modulated seasonality on absorbing BC aerosol trend estimates over the European Arctic.

The PSCF method, applied to backward simulations of a BC tracer and b_{abs} measurements, shows that the accumulated Cold period PSCF probabilities are largest over the northwestern part of Asia, followed by Europe, Eastern Asia, and North America, in decreasing order. In previous similar studies (Eleftheriadis et al., 2009; Hirdman, Sodemann, et al., 2010), Europe appeared less influential and Siberia dominant in the eBC high quantiles. It is also concluded that the combined assessment of the long observation record of aerosol absorbing carbon at the Zeppelin station and detailed transport modeling, is displaying a clearer than previously found influence of the large-scale circulation patterns active in this area of the High Arctic. Regarding the spatial variability of the contributing regions to the observed aerosol light absorption, the gas flaring emissions in Siberia, North Sea, Alberta, and Nova Scotia are quite well captured, as the PSCF seasonal maps mirror the BC emission source areas from different source types displayed in Stohl et al. (2013). An important finding of this study is that the BC arriving in the European High Arctic is greatly affected during the colder period of the year by the sign of the SCAN index. During the Warm period, the extent of influence of the BC Eurasian source regions is limited to latitudes higher than 60°N, when NAO is positive or SCAN is negative. The latter is more pronounced for the European source regions.

These findings allow a better quantified estimate of the fate of emissions over the years in the Northern Hemisphere and a better assessment of their influence in the observed BC metrics in the Artic, in this case the b_{abs}. The circulation patterns appear to induce a long-term modulation which is also found to have consistent regional features. Ongoing climate change and disturbance of these features must be taken into account in the long-term trend analysis on the Arctic aerosol optical properties and BC concentrations.

Data Availability Statement

Atmospheric indices data can be found at: https://www.cpc.ncep.noaa.gov/data/teledoc/telecontents.shtml. The reader can obtain all the data supporting the conclusions of this work at the following public weblinks: https://zenodo.org/record/5036451, https://zenodo.org/record/4926452, https://zenodo.org/record/4927585,

https://zenodo.org/record/4942618, https://zenodo.org/record/4943929, https://zenodo.org/record/4944979, https://zenodo.org/record/4945769, https://zenodo.org/record/4954128, https://zenodo.org/record/4954540, https://zenodo.org/record/4955999, https://zenodo.org/record/4963948, https://zenodo.org/record/4964787, https://zenodo.org/record/4965124, https://zenodo.org/record/4966330, https://zenodo.org/record/4971672, and https://zenodo.org/record/4972849.

Acknowledgments
The authors acknowledge the support by the Norwegian Polar Institute for the instruments running at the Zeppelin station as well as Kjetil Tørseth, Markus Fiebig, and Ove Hermansen for their support and fruitful discussions over the years regarding the content of this work. This project has received funding from the European Union's Horizon 2020 research and innovation program under grant agreement no. 689443 via project iCUPE (Integrative and Comprehensive Understanding on Polar Environments) and through ACTRIS2 (654109). The authors would like to thank the Climate Prediction Center (CPC) at the National Weather Service (NWS), USA, for providing atmospheric indices data.

References

Bacer, S., Christoudias, T., & Pozzer, A. (2016). Projection of North Atlantic Oscillation and its effect on tracer transport. *Atmospheric Chemistry and Physics*, *16*(24), 15581. https://doi.org/10.5194/acp-16-15581-2016

Backman, J., Schmeisser, L., & Asmi, E. (2021). Asian emissions explain much of the arctic black carbon events. *Geophysical Research Letters*, *48*(5), e2020GL091913. https://doi.org/10.1029/2020GL091913

Backman, J., Schmeisser, L., Virkkula, A., Ogren, J. A., Asmi, E., Starkweather, S., et al. (2017). On aethalometer measurement uncertainties and an instrument correction factor for the arctic. *Atmospheric Measurement Techniques*, *10*(12), 5039–5062. https://doi.org/10.5194/amt-10-5039-2017

Barnston, A. G., & Livezey, R. E. (1987). Classification, seasonality and persistence of low-frequency atmospheric circulation patterns. *Monthly Weather Review*, *115*(6), 1083–1126. https://doi.org/10.1175/1520-0493(1987)115<1083:CSAPOL>2.0.CO;2

Bond, T. C., Doherty, S. J., Fahey, D. W., Forster, P. M., Berntsen, T., DeAngelo, B. J., et al. (2013). Bounding the role of black carbon in the climate system: A scientific assessment. *Journal of Geophysical Research: Atmospheres*, *118*(11), 5380–5552. https://doi.org/10.1002/jgrd.50171

Bourgeois, Q., & Bey, I. (2011). Pollution transport efficiency toward the Arctic: Sensitivity to aerosol scavenging and source regions. *Journal of Geophysical Research*, *116*(D8), D08213. https://doi.org/10.1029/2010JD015096

Breider, T. J., Mickley, L. J., Jacob, D. J., Ge, C., Wang, J., Payer Sulprizio, M., et al. (2017). Multidecadal trends in aerosol radiative forcing over the Arctic: Contribution of changes in anthropogenic aerosol to Arctic warming since 1980. *Journal of Geophysical Research: Atmospheres*, *122*(6), 3573–3594. https://doi.org/10.1002/2016JD025321

Bueh, C., & Nakamura, H. (2007). Scandinavian pattern and its climatic impact. *Quarterly Journal of the Royal Meteorological Society: A Journal of the Atmospheric Sciences, Applied Meteorology and Physical Oceanography*, *133*(629), 2117–2131. https://doi.org/10.1002/qj.173

Callaghan, T. V., Johansson, M., Brown, R. D., Groisman, P. Y., Labba, N., Radionov, V., et al. (2011). The changing face of Arctic snow cover: A synthesis of observed and projected changes. *Ambio*, *40*(1), 17–31. https://doi.org/10.1007/s13280-011-0212-y

Casadio, S., Arino, O., & Serpe, D. (2012). Gas flaring monitoring from space using the ATSR instrument series. *Remote Sensing of Environment*, *116*, 239–249. https://doi.org/10.1016/j.rse.2010.11.022

Christoudias, T., Pozzer, A., & Lelieveld, J. (2012). Influence of the North Atlantic Oscillation on air pollution transport. *Atmospheric Chemistry and Physics*, *12*(2), 869–877. https://doi.org/10.5194/acp-12-869-2012

Collaud Coen, M., Andrews, E., Alastuey, A., Arsov, T. P., Backman, J., Brem, B. T., et al. (2020). Multidecadal trend analysis of in situ aerosol radiative properties around the world. *Atmospheric Chemistry and Physics*, *20*(14), 8867–8908. https://doi.org/10.5194/acp-20-8867-2020

Eckhardt, S., Quennehen, B., Olivié, D. J. L., Berntsen, T. K., Cherian, R., Christensen, J. H., et al. (2015). Current model capabilities for simulating black carbon and sulfate concentrations in the arctic atmosphere: A multi-model evaluation using a comprehensive measurement data set. *Atmospheric Chemistry and Physics*, *15*(16), 9413–9433. https://doi.org/10.5194/acp-15-9413-2015

Eckhardt, S., Stohl, A., Beirle, S., Spichtinger, N., James, P., Forster, C., et al. (2003). The north Atlantic oscillation controls air pollution transport to the arctic. *Atmospheric Chemistry and Physics*, *3*(5), 1769–1778. https://doi.org/10.5194/acp-3-1769-2003

Eleftheriadis, K., Nyeki, S., Psomiadou, C., & Colbeck, I. (2004). Background aerosol properties in the european arctic. *Water, Air, and Soil Pollution: Focus*, *4*(4–5), 23–30. https://doi.org/10.1023/B:WAFO.0000044783.70114.19

Eleftheriadis, K., Vratolis, S., & Nyeki, S. (2009). Aerosol black carbon in the European Arctic: Measurements at Zeppelin station, Ny-Ålesund, Svalbard from 1998–2007. *Geophysical Research Letters*, *36*(2), L02809. https://doi.org/10.1029/2008GL035741

Folland, C. K., Knight, J., Linderholm, H. W., Fereday, D., Ineson, S., & Hurrel, J. W. (2009). The summer north Atlantic oscillation: Past, present, and future. *Journal of Climate*, *22*(5), 1082–1103. https://doi.org/10.1175/2008JCLI2459.1

Garrett, T. J., Zhao, C., Dong, X., Mace, G. G., & Hobbs, P. V. (2004). Effects of varying aerosol regimes on low-level Arctic stratus. *Geophysical Research Letters*, *31*(17), L17105. https://doi.org/10.1029/2004GL019928

Giglio, L., Randerson, J. T., & Van Der Werf, G. R. (2013). Analysis of daily, monthly, and annual burned area using the fourth-generation global fire emissions database (GFED4). *Journal of Geophysical Research: Biogeosciences*, *118*(1), 317–328. https://doi.org/10.1002/jgrg.20042

Hadley, O. L., & Kirchstetter, T. W. (2012). Black-carbon reduction of snow albedo. *Nature Climate Change*, *2*(6), 437–440. https://doi.org/10.1038/NCLIMATE1433

Hirdman, D., Burkhart, J. F., Sodemann, H., Eckhardt, S., Jefferson, A., Quinn, P. K., & Stohl, A. (2010). Long-term trends of black carbon and sulphate aerosol in the Arctic: Changes in atmospheric transport and source region emissions. *Atmospheric Chemistry and Physics*, *10*(19), 9351–9368. https://doi.org/10.5194/acp-10-9351-2010

Hirdman, D., Sodemann, H., Eckhardt, S., Burkhart, J. F., Jefferson, A., Mefford, T., et al. (2010). Source identification of short-lived air pollutants in the Arctic using statistical analysis of measurement data and particle dispersion model output. *Atmospheric Chemistry and Physics*, *10*(2), 669–693. https://doi.org/10.5194/acp-10-669-2010

Holopainen, E., Kokkola, H., Laakso, A., & Kühn, T. (2020). In-cloud scavenging scheme for sectional aerosol modules - Implementation in the framework of the sectional aerosol module for large scale applications version 2.0 (SALSA2.0) global aerosol module. *Geoscientific Model Development*, *13*(12), 6215–6235. https://doi.org/10.5194/gmd-13-6215-2020

Huang, K., & Fu, J. S. (2016). A global gas flaring black carbon emission rate dataset from 1994 to 2012. *Scientific data*, *3*(1), 1–11. https://doi.org/10.1038/sdata.2016.104

Hurrell, J. W. (1995). Decadal trends in the North Atlantic Oscillation: Regional temperatures and precipitation. *Science*, *269*(5224), 676–679. https://doi.org/10.1126/science.269.5224.676

Hurrell, J. W., Kushnir, Y., Ottersen, G., & Visbeck, M. (2003). *An overview of the north Atlantic oscillation*. https://doi.org/10.1029/134GM01

Hyvärinen, A. P., Kolmonen, P., Kerminen, V. M., Virkkula, A., Leskinen, A., Komppula, M., et al. (2011). Aerosol black carbon at five background measurement sites over Finland, a gateway to the Arctic. *Atmospheric Environment*, *45*(24), 4042–4050. https://doi.org/10.1016/j.atmosenv.2011.04.026

Jacobi, H.-W., Obleitner, F., Da Costa, S., Ginot, P., Eleftheriadis, K., Aas, W., & Zanatta, M. (2019). Deposition of ionic species and black carbon to the Arctic snowpack: Combining snow pit observations with modeling. *Atmospheric Chemistry and Physics*, *19*, 10361–10377. https://doi.org/10.5194/acp-19-10361-2019

Kahnert, M., & Kanngießer, F. (2020). Modelling optical properties of atmospheric black carbon aerosols. *Journal of Quantitative Spectroscopy and Radiative Transfer*, *244*, 106849. https://doi.org/10.1016/j.jqsrt.2020.106849

Klimont, Z., Kupiainen, K., Heyes, C., Purohit, P., Cofala, J., Rafaj, P., et al. (2017). Global anthropogenic emissions of particulate matter including black carbon. *Atmospheric Chemistry and Physics*, *17*(14), 8681–8723. https://doi.org/10.5194/acp-17-8681-2017

Laj, P., Bigi, A., Rose, C., Andrews, E., Lund Myhre, C., Collaud Coen, M., et al. (2020). A global analysis of climate-relevant aerosol properties retrieved from the network of global atmosphere watch (GAW) near-surface observatories. *Atmospheric Measurement Techniques*, *13*(8), 4353–4392. https://doi.org/10.5194/amt-13-4353-2020

Liu, D., He, C., & SchwarzWang, J. P. X. (2020). Lifecycle of light-absorbing carbonaceous aerosols in the atmosphere. *npj Climate and Atmospheric Science*, *3*, 40. https://doi.org/10.1038/s41612-020-00145-8

Lund, M. T., Samset, B. H., Skeie, R. B., Watson-Parris, D., Katich, J. M., Schwarz, J. P., & Weinzierl, B. (2018). Short black carbon lifetime inferred from a global set of aircraft observations. *Npj Climate and Atmospheric Science*, *1*(1), 31. https://doi.org/10.1038/s41612-018-0040-x

Marelle, L., Raut, J. C., Law, K. S., & Duclaux, O. (2018). Current and future Arctic aerosols and ozone from remote emissions and emerging local sources—Modeled source contributions and radiative effects. *Journal of Geophysical Research: Atmospheres*, *123*(22), 12–942. https://doi.org/10.1029/2018JD028863

Ohata, S., Mori, T., Kondo, Y., Sharma, S., Hyvärinen, A., Andrews, E., et al. (2021). Estimates of mass absorption cross sections of black carbon for filter-based absorption photometers in the Arctic (preprint). *Atmospheric Measurement Techniques Discussion*. https://doi.org/10.5194/amt-2021-166

Petäjä, T., Duplissy, E., Tabakova, K., Schmale, J., Altstädter, B., Ancellet, G., et al. (2020). Overview: Integrative and comprehensive understanding on polar environments (iCUPE)-concept and initial results. *Atmospheric Chemistry and Physics*, *20*(14), 8551–8592. https://doi.org/10.5194/acp-20-8551-2020

Polissar, A. V., Hopke, P. K., & Harris, J. M. (2001). Source regions for atmospheric aerosol measured at barrow, Alaska. *Environmental Science and Technology*, *35*(21), 4214–4226. https://doi.org/10.1021/es0107529

Popovicheva, O., Diapouli, E., Makshtas, A., Shonija, N., Manousakas, M., Saraga, D., et al. (2019). East Siberian Arctic background and black carbon polluted aerosols at HMO Tiksi. *Science of the Total Environment*, *655*, 924–938. https://doi.org/10.1016/j.scitotenv.2018.11.165

Popovicheva, O. B., Evangeliou, N., Eleftheriadis, K., Kalogridis, A.-C., Sitnikov, N., Eckhardt, S., & Stohl, A. (2017). *Environmental Science & Technology*, *51*(7), 3871–3879. https://doi.org/10.1021/acs.est.6b05832

Pozzoli, L., Dobricic, S., Russo, S., & Vignati, E. (2017). Impacts of large-scale atmospheric circulation changes in winter on black carbon transport and deposition to the Arctic. *Atmospheric Chemistry and Physics*, *17*(19), 11803. https://doi.org/10.5194/acp-17-11803-2017

Qi, L., Li, Q., Henze, D. K., Tseng, H. -, & He, C. (2017). Sources of springtime surface black carbon in the arctic: An adjoint analysis for April 2008. *Atmospheric Chemistry and Physics*, *17*(15), 9697–9716. https://doi.org/10.5194/acp-17-9697-2017

Quaas, J. (2011). Global warming: The soot factor. *Nature*, *471*(7339), 456–457. https://doi.org/10.1038/471456a

Sand, M., Samset, B. H., Balkanski, Y., Bauer, S., Bellouin, N., Berntsen, T. K., & Ghan, S. J. (2017). Aerosols at the Poles: An AeroCom phase II multi-model evaluation. *Atmospheric Chemistry and Physics*, *17*(19), 12197–12218. https://doi.org/10.5194/acp-17-12197-2017

Schmeisser, L., Backman, J., Ogren, J. A., Andrews, E., Asmi, E., Starkweather, S., et al. (2018). Seasonality of aerosol optical properties in the arctic. *Atmospheric Chemistry and Physics*, *18*(16), 11599–11622. https://doi.org/10.5194/acp-18-11599-2018

Seinfeld, J. (2008). Atmospheric science: Black carbon and brown clouds. *Nature Geoscience*, *1*(1), 15–16. https://doi.org/10.1038/ngeo.2007.62

Sharma, S., Ishizawa, M., Chan, D., Lavoué, D., Andrews, E., Eleftheriadis, K., & Maksyutov, S. (2013). 16-year simulation of arctic black carbon: Transport, source contribution, and sensitivity analysis on deposition. *Journal of Geophysical Research: Atmospheres*, *118*(2), 943–964. https://doi.org/10.1029/2012JD017774

Shindell, D. T., Chin, M., Dentener, F., Doherty, R. M., Faluvegi, G., Fiore, A. M., et al. (2008). A multi-model assessment of pollution transport to the arctic. *Atmospheric Chemistry and Physics*, *8*(17), 5353–5372. https://doi.org/10.5194/acp-8-5353-2008

Stohl, A., Forster, C., Frank, A., Seibert, P., & Wotawa, G. (2005). Technical note: The lagrangian particle dispersion model FLEXPART version 6.2. *Atmospheric Chemistry and Physics*, *5*(9), 2461–2474. https://doi.org/10.5194/acp-5-2461-2005

Stohl, A., Klimont, Z., Eckhardt, S., Kupiainen, K., Shevchenko, V. P., Kopeikin, V. M., & Novigatsky, A. N. (2013). Black carbon in the arctic: The underestimated role of gas flaring and residential combustion emissions. *Atmospheric Chemistry and Physics*, *13*(17), 8833–8855. https://doi.org/10.5194/acp-13-8833-2013

Stone, R. S., Sharma, S., Herber, A., Eleftheriadis, K., & Nelson, D. W. (2014). A characterization of arctic aerosols on the basis of aerosol optical depth and black carbon measurements. *Elementa*, *2*. https://doi.org/10.12952/journal.elementa.000027

Winiger, P., Andersson, A., Eckhardt, S., Stohl, A., & Gustafsson, O. (2016). The sources of atmospheric black carbon at a European gateway to the arctic. *Nature Communications*, *7*, 12776. https://doi.org/10.1038/ncomms12776

Winiger, P., Andersson, A., Eckhardt, S., Stohl, A., Semiletov, I. P., Dudarev, O. V., et al. (2017). Siberian arctic black carbon sources constrained by model and observation. *Proceedings of the National Academy of Sciences of the United States of America*, *114*(7), E1054–E1061. https://doi.org/10.1073/pnas.1613401114

Zanatta, M., Laj, P., Gysel, M., Baltensperger, U., Vratolis, S., Eleftheriadis, K., et al. (2018). Effects of mixing state on optical and radiative properties of black carbon in the European arctic. *Atmospheric Chemistry and Physics*, *18*(19), 14037–14057. https://doi.org/10.5194/acp-18-14037-2018